




Universal T -linear resistivity and Planckian dissipation in overdoped cuprates

A. Legros^{1,2}, S. Benhabib³, W. Tabis^{3,4}, F. Laliberté¹ , M. Dion¹, M. Lizaire¹, B. Vignolle³, D. Vignolles^{1,3} , H. Raffy⁵, Z. Z. Li⁵, P. Auban-Senzier⁵, N. Doiron-Leyraud¹, P. Fournier^{1,6}, D. Colson², L. Taillefer^{1,6*}  and C. Proust^{1,6*} 

The perfectly linear temperature dependence of the electrical resistivity observed as $T \rightarrow 0$ in a variety of metals close to a quantum critical point^{1–4} is a major puzzle of condensed-matter physics⁵. Here we show that T -linear resistivity as $T \rightarrow 0$ is a generic property of cuprates, associated with a universal scattering rate. We measured the low-temperature resistivity of the bilayer cuprate $\text{Bi}_2\text{Sr}_2\text{CaCu}_2\text{O}_{8+\delta}$ and found that it exhibits a T -linear dependence with the same slope as in the single-layer cuprates $\text{Bi}_2\text{Sr}_2\text{CuO}_{6+\delta}$ (ref. ⁶), $\text{La}_{1.6-x}\text{Nd}_{0.4}\text{Sr}_x\text{CuO}_4$ (ref. ⁷) and $\text{La}_{2-x}\text{Sr}_x\text{CuO}_4$ (ref. ⁸), despite their very different Fermi surfaces and structural, superconducting and magnetic properties. We then show that the T -linear coefficient (per CuO_2 plane), A_1^\square , is given by the universal relation $A_1^\square T_f = h/2e^2$, where e is the electron charge, h is the Planck constant and T_f is the Fermi temperature. This relation, obtained by assuming that the scattering rate $1/\tau$ of charge carriers reaches the Planckian limit^{9,10}, whereby $h/\tau = k_B T$, works not only for hole-doped cuprates^{6–8,11,12} but also for electron-doped cuprates^{13,14}, despite the different nature of their quantum critical point and strength of their electron correlations.

In conventional metals, the electrical resistivity $\rho(T)$ normally varies as T^2 in the limit $T \rightarrow 0$, where electron–electron scattering dominates, in accordance with Fermi-liquid theory. However, close to a quantum critical point (QCP) where a phase of antiferromagnetic order ends, $\rho(T) \sim T^n$, with $n < 2.0$. Most striking is the observation of a perfectly linear T dependence $\rho(T) = \rho_0 + A_1 T$ as $T \rightarrow 0$ in several very different materials, when tuned to their magnetic QCP; for example, the quasi-one-dimensional (1D) organic conductor $(\text{TMTSF})_2\text{PF}_6$ (ref. ⁴), the quasi-2D ruthenate $\text{Sr}_3\text{Ru}_2\text{O}_7$ (ref. ³) and the 3D heavy-fermion metal CeCu_6 (ref. ¹). This T -linear resistivity as $T \rightarrow 0$ has emerged as one of the major puzzles in the physics of metals⁵, and while several theoretical scenarios have been proposed¹⁵, no compelling explanation has been found.

In cuprates, a perfect T -linear resistivity as $T \rightarrow 0$ has been observed (once superconductivity is suppressed by a magnetic field) in two closely related electron-doped materials, $\text{Pr}_{2-x}\text{Ce}_x\text{CuO}_{4\pm\delta}$ (PCCO)^{2,16,17} and $\text{La}_{2-x}\text{Ce}_x\text{CuO}_4$ (LCCO)^{13,14}, and in three hole-doped materials: $\text{Bi}_2\text{Sr}_2\text{CuO}_{6+\delta}$ (ref. ⁶), $\text{La}_{2-x}\text{Sr}_x\text{CuO}_4$ (LSCO)⁸ and $\text{La}_{1.6-x}\text{Nd}_{0.4}\text{Sr}_x\text{CuO}_4$ (Nd-LSCO)^{7,11,12}. On the electron-doped side, T -linear resistivity is seen just above the QCP¹⁶ where antiferromagnetic order ends¹⁸ as a function of x , and as such it may not come as a surprise. On the hole-doped side, however, the doping values

where $\rho(T) = \rho_0 + A_1 T$ as $T \rightarrow 0$ are very far from the QCP where long-range antiferromagnetic order ends ($p_N \sim 0.02$); for example, at $p = 0.24$ in Nd-LSCO (Fig. 1a) and in the range $p = 0.21–0.26$ in LSCO (Fig. 1b). Instead, these values are close to the critical doping where the pseudogap phase ends (that is, at $p^* = 0.23 \pm 0.01$ in Nd-LSCO (ref. ¹¹) and at $p^* \sim 0.18–0.19$ in LSCO (ref. ⁸)), where the role of antiferromagnetic spin fluctuations is not clear. In $\text{Bi}2201$, p^* is farther still (see Supplementary Section 10).

To make progress, several questions must be answered. Is T -linear resistivity as $T \rightarrow 0$ in hole-doped cuprates limited to single-layer materials with low T_c or is it generic? Why is $\rho(T) = \rho_0 + A_1 T$ as $T \rightarrow 0$ seen in LSCO over an anomalously wide doping range⁸? Is there a common mechanism linking cuprates to the other metals where $\rho \sim T$ as $T \rightarrow 0$?

To establish the universal character of T -linear resistivity in cuprates, we have turned to $\text{Bi}_2\text{Sr}_2\text{CaCu}_2\text{O}_{8+\delta}$ ($\text{Bi}2212$). While Nd-LSCO and LSCO have essentially the same single electron-like diamond-shaped Fermi surface at $p > p^*$ (refs ^{19,20}), $\text{Bi}2212$ has a very different Fermi surface, consisting of two sheets, one of which is also diamond-like at $p > 0.22$, but the other is much more circular²¹ (see Supplementary Section 1). Moreover, the structural, magnetic and superconducting properties of $\text{Bi}2212$ are very different to those of Nd-LSCO and LSCO: a stronger 2D character, a larger gap to spin excitations, no spin-density-wave order above $p \sim 0.1$ and a much higher superconducting T_c .

We measured the resistivity of $\text{Bi}2212$ at $p = 0.23$ by suppressing superconductivity with a magnetic field of up to 58 T. At $p = 0.23$, the system is just above its pseudogap critical point ($p^* = 0.22$ (ref. ²²); see Supplementary Section 2). Our data are shown in Fig. 2. The raw data at $H = 55$ T reveal a perfectly linear T dependence of $\rho(T)$ down to the lowest accessible temperature (Fig. 1a). Correcting for the magnetoresistance (see Methods and Supplementary Section 3), as was done for LSCO (ref. ⁸), we find that the T -linear dependence of $\rho(T)$ seen in $\text{Bi}2212$ at $H = 0$ from $T \sim 120$ K down to T_c simply continues to low temperature, with the same slope $A_1 = 0.62 \pm 0.06 \mu\Omega \text{ cm K}^{-1}$ (Fig. 2b). Measured per CuO_2 plane, this gives $A_1^\square \equiv A_1/d = 8.0 \pm 0.9 \Omega \text{ K}^{-1}$, where d is the (average) separation between CuO_2 planes. Remarkably, this is the same value, within error bars, as measured in Nd-LSCO at $p = 0.24$, where $A_1^\square = 7.4 \pm 0.8 \Omega \text{ K}^{-1}$ (see Table 1).

The observation of T -linear resistivity in those two cuprates shows that it is robust against changes in the shape, topology and

¹Institut Quantique, Département de Physique & RQMP, Université de Sherbrooke, Sherbrooke, Québec, Canada. ²SPEC, CEA, CNRS-UMR 3680, Université Paris-Saclay, Gif sur Yvette Cedex, France. ³Laboratoire National des Champs Magnétiques Intenses (CNRS, EMFL, INSA, UJF, UPS), Toulouse, France. ⁴AGH University of Science and Technology, Faculty of Physics and Applied Computer Science, Krakow, Poland. ⁵Laboratoire de Physique des Solides, Université Paris-Sud, Université Paris-Saclay, CNRS UMR 8502, Orsay, France. ⁶Canadian Institute for Advanced Research, Toronto, Ontario, Canada. *e-mail: louis.taillefer@usherbrooke.ca; cyril.proust@lncmi.cnrs.fr

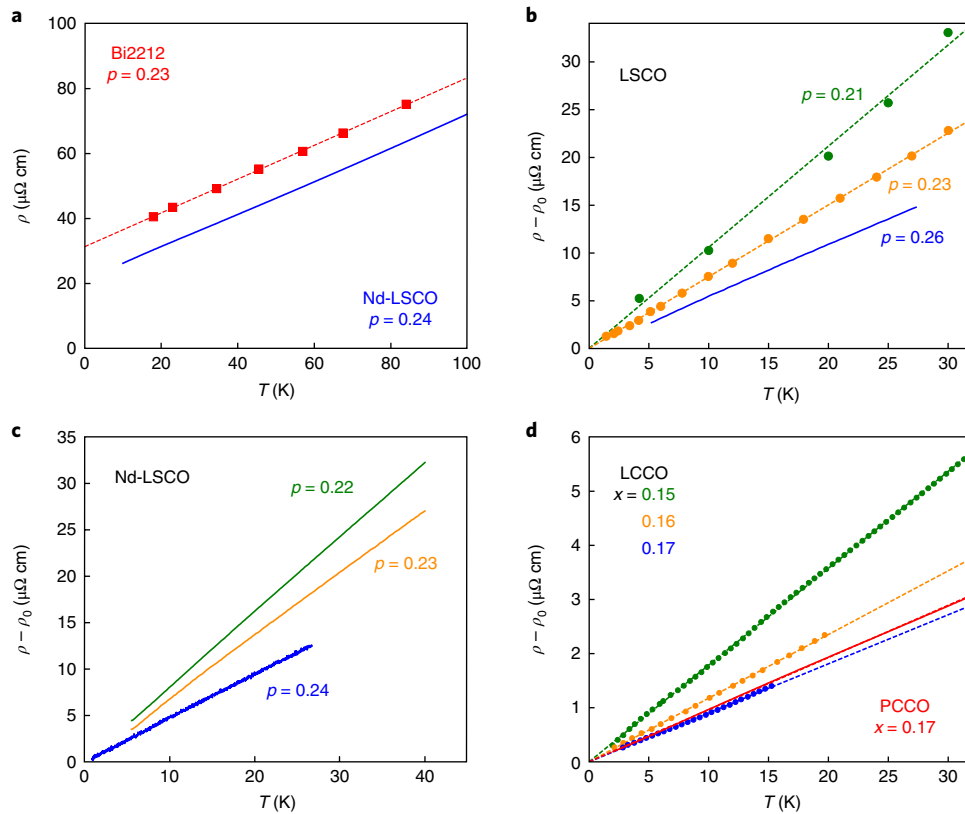


Fig. 1 | T-linear resistivity in five overdoped cuprates. In-plane electrical resistivity ρ of cuprates showing a T -linear resistivity at low temperature. **a**, Nd-LSCO at $p=0.24$ (blue, $H=16$ T; from ref.¹¹) and Bi2212 at $p=0.23$ (red squares, $H=55$ T; this work, Fig. 2a). **b**, Temperature-dependent part of the resistivity, $\rho(T) - \rho_0$, for LSCO at $p=0.21$ (green, $H=48$ T; from ref.⁸), $p=0.23$ (orange, $H=48$ T; from ref.⁸), $p=0.26$ (blue, $H=18$ T; from ref.⁴²) (see Supplementary Section 7). **c**, $\rho(T) - \rho_0$ for Nd-LSCO at $H=33$ T, at $p=0.22$ (green) and $p=0.23$ (orange) (from ref.¹²) and at $p=0.24$ (blue; from ref.⁷). For $p=0.22$ and 0.23 , a pressure of 2 GPa was applied to suppress the pseudogap phase (see Supplementary Section 4). **d**, $\rho(T) - \rho_0$ for LCCO at $x=0.15$ (green, $H=8$ T), $x=0.16$ (orange, $H=6.5$ T) and $x=0.17$ (blue, $H=4$ T) (from ref.¹⁴), and PCCO at $x=0.17$ (red, $H=16$ T; this work, see Supplementary Section 5). All dashed lines are a linear fit.

multiplicity of the Fermi surface. By contrast, the Hall coefficient R_H is not. In Fig. 2d, we compare $R_H(T)$ in Bi2212 and in Nd-LSCO (and PCCO). We see strong differences, brought about by the different anisotropies in either the inelastic scattering or the Fermi surface, or both²³. Nevertheless, $\rho(T)$ is perfectly linear in both cases. Moreover, the coefficient A_1^\square is the same despite the very different spectra of low-energy spin fluctuations, gapped in Bi2212 (ref.²⁴) and ungapped in Nd-LSCO (ref.²⁵). We conclude that a T -linear resistivity as $T \rightarrow 0$ is a generic and robust property of cuprates.

Note that $\rho(T)$ deviates from pure T -linearity above a certain temperature, and in this high- T regime a generic evolution has also been found in LSCO (ref.²⁶), with $\rho(T) \sim A_1 T + A_2 T^2$. Here we focus strictly on the low- T regime of pure T -linear resistivity (see Supplementary Section 12). In this regime, and close to the QCP of $\text{BaFe}_2(\text{As}_{1-x}\text{P}_x)_2$ (at $x=0.31$), an empirical scaling relationship between applied magnetic field and temperature has been proposed²⁷, but this scaling does not work very well in Bi2212 (see Supplementary Section 11).

We now investigate the strength of the T -linear resistivity; that is, the magnitude of A_1 . In Fig. 3b, we plot A_1^\square versus p for hole-doped cuprates. We see from the LSCO data⁸ that A_1^\square increases with decreasing p (Fig. 1b), from $A_1^\square \sim 8 \Omega \text{K}^{-1}$ at $p=0.26$ to $A_1^\square \sim 15 \Omega \text{K}^{-1}$ at $p=0.21$ (see Supplementary Table 2 in Supplementary Section 13 and Methods). In Nd-LSCO, we see a similar increase (Figs. 1c and 3b), when pressure¹² is used to suppress the onset of the pseudogap at $p=0.22$ and $p=0.23$ (see Supplementary Section 4). In Fig. 1d, we present our data on PCCO at $x=0.17$ (see also Supplementary

Section 5), and compare with previous data on LCCO (ref.¹⁴; Supplementary Section 6). In Fig. 4b, we plot A_1^\square versus x for electron-doped cuprates, and see that A_1^\square also increases with decreasing x , from $A_1^\square \sim 1.5 \Omega \text{K}^{-1}$ at $x=0.17$ to $A_1^\square \sim 3 \Omega \text{K}^{-1}$ at $x=0.15$ (see Supplementary Table 4 in Supplementary Section 13 and Methods). Note that these values are five times smaller than in hole-doped cuprates.

To summarize: A_1^\square increases as the doping is reduced in both hole-doped and electron-doped cuprates; A_1^\square is much larger in hole-doped cuprates; T -linear resistivity as $T \rightarrow 0$ is observed over a range of doping, not just at one doping; T -linear resistivity does not depend on the nature of the inelastic scattering process (hole-doped versus electron-doped) or on the topology of the Fermi surface (LSCO versus NCCO, Bi2212 versus Nd-LSCO; Supplementary Section 1).

To explain these experimental facts, we consider the empirical observation that the strength of the T -linear resistivity for several metals is approximately given by a scattering rate that has a universal value, namely $\hbar/\tau = k_B T$ (ref.¹⁰), and test it in cuprates. This observation suggests that a T -linear regime will be observed whenever $1/\tau$ reaches its Planckian limit, $k_B T/\hbar$, irrespective of the underlying mechanism for inelastic scattering⁹. In the following, we use a standard Fermi-liquid approach to extract effective masses and inelastic scattering rates, as in ref.¹⁰. In the simple case of an isotropic Fermi surface, the connection between ρ and τ is given by the Drude formula, $\rho = (m^*/ne^2) (1/\tau)$, where n is the carrier density and m^* is the effective mass. Thus, when $\rho(T) = \rho_0 + A_1 T$, then

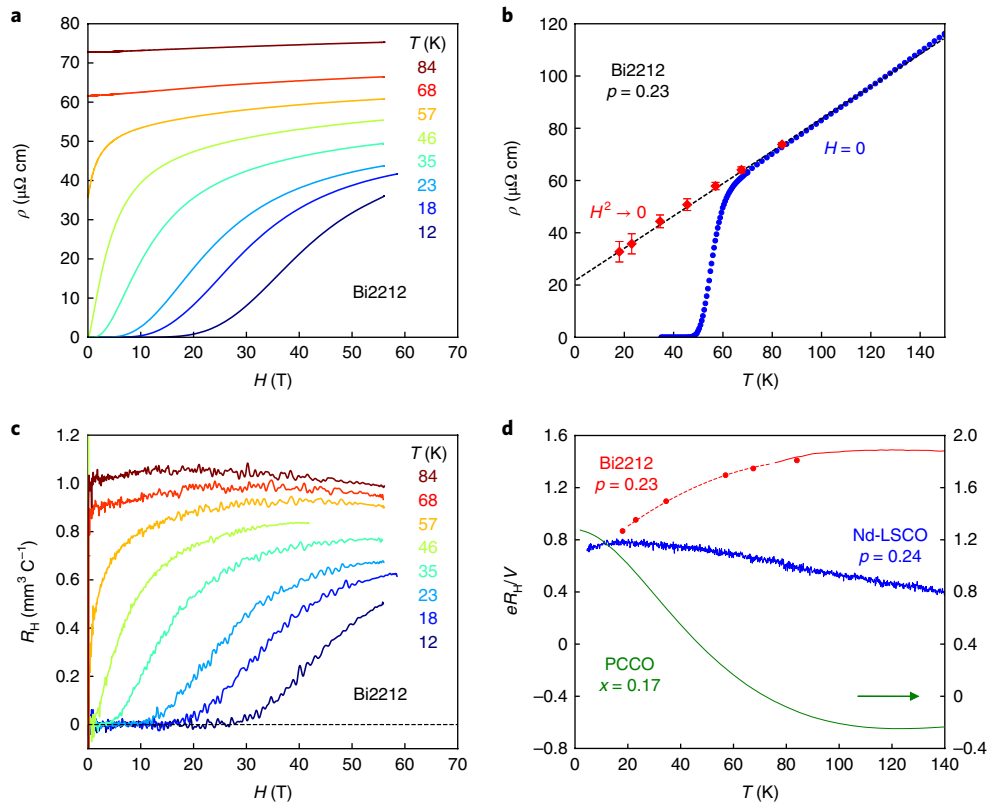


Fig. 2 | Resistivity and Hall coefficient of our Bi2212 film. **a**, Resistivity of our Bi2212 film with $p=0.23$ as a function of magnetic field, at the indicated temperatures. The value of ρ at $H=55$ T is plotted versus T in Supplementary Fig. 3b of Supplementary section 3. **b**, Resistivity as a function of temperature, at $H=0$ (blue). The red diamonds are high-field data extrapolated to zero field by fitting $\rho(H)$ to $a + bH^2$ (see Methods and Supplementary Section 3). The error bars are estimated by the difference $[\rho(H=55 \text{ T}) - \rho(H^2 \rightarrow 0)]/2$. The dashed line is a linear fit to the red diamonds. **c**, Hall coefficient of our Bi2212 film as a function of magnetic field, at the indicated temperatures. The value of R_H at $H=55$ T is plotted versus T in **d**. **d**, Hall coefficient as a function of temperature for three cuprates, plotted as eR_H/V , where e is the electron charge and V is the volume per Cu atom: Bi2212 at $p=0.23$ (red curve, $H=9$ T; red dots, $H=55$ T, **c**); Nd-LSCO at $p=0.24$ (blue, $H=16$ T; from ref.¹¹); PCCO at $x=0.17$ (green, $H=15$ T, right axis; from ref.⁴¹). The red dashed line is a guide to the eye.

$A_1 = (m^*/n e^2)(1/\tau)(1/T) = \alpha(m^*/n)(k_B/e^2\hbar)$, with $\hbar/\tau \equiv \alpha k_B T$. In two dimensions, this can be written succinctly as:

$$A_1^\square = \alpha (h/2e^2) 1/T_F \quad (1)$$

where $T_F = (\pi\hbar^2/k_B)(nd/m^*)$ is the Fermi temperature.

Let us first evaluate α in electron-doped cuprates, where the Drude formula is expected to work well, since their single Fermi surface is highly 2D and circular (in the overdoped region²⁸; see Supplementary Section 1). Quantum oscillations in $\text{Nd}_{2-x}\text{Ce}_x\text{CuO}_4$ (NCCO) provide a direct and precise measurement of n and m^* in electron-doped cuprates^{29,30}. The Luttinger rule sets the carrier density to be $n = (1-x)/(a^2d)$, given precisely by the oscillation frequency $F = nd(h/2e)$, where x is the number of doped electrons per Cu atom and a is the in-plane lattice constant. In Fig. 4a, we see that m^* increases from $2.3 m_0$ at $x=0.173$ to $3.0 m_0$ at $x=0.151$, where m_0 is the bare electron mass (see Supplementary Table 3 in Supplementary Section 13 and Methods). This increasing value is consistent, within error bars, with specific heat data in PCCO at $x=0.15$, where $\gamma = 5.5 \pm 0.4 \text{ mJ K}^{-2} \text{ mol}^{-1}$ (ref.³¹), which yields $m^* = 3.6 \pm 0.3 m_0$ (see equation (2) below). We use n and m^* to estimate T_F and then plot, in Fig. 4b, the value of A_1^\square predicted by equation (1), for $\alpha=1$ (solid line in Fig. 4b; Supplementary Table 3 in Supplementary Section 13). Comparison with the measured values of A_1^\square in PCCO (red hexagon in Fig. 4b) and in LCCO (blue circles in Fig. 4b), listed in Supplementary Table 4

(see Supplementary Section 13 and Methods), shows that the scattering rate in electron-doped cuprates is given by $\hbar/\tau = \alpha k_B T$, with $\alpha = 1.0 \pm 0.3$; that is, the Planckian limit is observed, within experimental error bars.

Let us now turn to hole-doped cuprates. Here our quantitative estimates will be more approximate, since Fermi surfaces are not circular but diamond-shaped (Supplementary Section 1), but we are looking for a large effect (factor ~ 5 in A_1^\square relative to electron-doped materials) and a qualitative trend (increase in A_1^\square as p is reduced towards p^*). In the absence of quantum oscillation data for Bi2212, LSCO, Nd-LSCO and Bi2201, we estimate m^* from specific heat data, since in two dimensions the specific heat coefficient γ is directly related to m^* :

$$\gamma = (\pi N_A k_B^2 / 3\hbar^2) a^2 m^* \quad (2)$$

for a single Fermi surface, where N_A is Avogadro's number. This connection between m^* and γ was nicely confirmed by quantum oscillations in $\text{Tl}_2\text{Ba}_2\text{CuO}_{6+\delta}$ at $p \sim 0.3$, where $m^* = 5.2 \pm 0.4 m_0$ and $\gamma = 7 \pm 1 \text{ mJ K}^{-2} \text{ mol}^{-1}$ (ref.³²). In Bi2212, $\gamma = 12 \pm 2 \text{ mJ K}^{-2}$ per mol-Cu at $p=0.22=p^*$ (ref.³³; see Supplementary Section 8), giving $m^* = 8.4 \pm 1.6 m_0$ (equation (2)). Applying equation (1), with $n(a^2d) = 1-p = 0.77$ (for an electron-like Fermi surface; Supplementary Section 1), the Planckian limit predicts $A_1^\square = 7.4 \pm 1.4 \Omega \text{ K}^{-1}$, while we measured $A_1^\square = 8.0 \pm 0.9 \Omega \text{ K}^{-1}$, so that $\alpha = 1.1 \pm 0.3$ (Table 1).

Table 1 | Slope of T -linear resistivity versus Planckian limit in seven materials

Material	Doping ^a	n (10^{27} m^{-3})	m^* (m_0)	A_1/d ($\Omega \text{ K}^{-1}$)	$h/(2e^2T_F)$ ($\Omega \text{ K}^{-1}$)	α
Bi2212	$p=0.23$	6.8	8.4 ± 1.6	8.0 ± 0.9	7.4 ± 1.4	1.1 ± 0.3
Bi2201	$p \sim 0.4$	3.5	7 ± 1.5	8 ± 2	8 ± 2	1.0 ± 0.4
LSCO	$p=0.26$	7.8	9.8 ± 1.7	8.2 ± 1.0	8.9 ± 1.8	0.9 ± 0.3
Nd-LSCO	$p=0.24$	7.9	12 ± 4	7.4 ± 0.8	10.6 ± 3.7	0.7 ± 0.4
PCCO	$x=0.17$	8.8	2.4 ± 0.1	1.7 ± 0.3	2.1 ± 0.1	0.8 ± 0.2
LCCO	$x=0.15$	9.0	3.0 ± 0.3	3.0 ± 0.45	2.6 ± 0.3	1.2 ± 0.3
TMTSF	$P=11 \text{ kbar}$	1.4	1.15 ± 0.2	2.8 ± 0.3	2.8 ± 0.4	1.0 ± 0.3

^aPressure in the case of TMTSF (last row). Comparison of the measured slope of the T -linear resistivity in the $T=0$ limit, A_1 , with the value predicted by the Planckian limit (equation (1); penultimate column), for four hole-doped cuprates (Bi2212, Bi2201, LSCO and Nd-LSCO), two electron-doped cuprates (PCCO and LCCO) and the organic conductor (TMTSF)₂PF₆, as discussed in the text (and Supplementary Information). The ratio α of the experimental value, $A_1^{\square}=A_1/d$, over the predicted value, is given in the last column. Although A_1^{\square} varies by a factor of 5, the ratio m^*/n , proportional to $1/T_F$, is seen to vary by the same amount, so that $\alpha=1.0$ in all cases, within error bars.

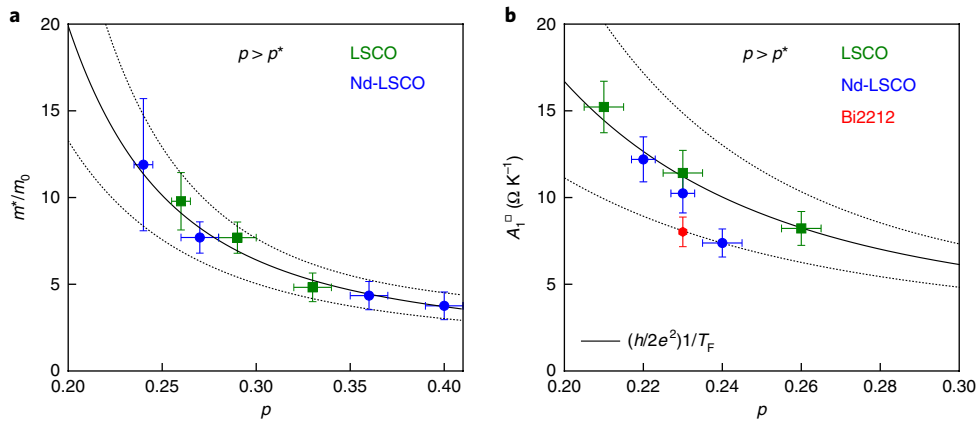


Fig. 3 | Effective mass m^* and slope of T -linear resistivity A_1^{\square} versus p in hole-doped cuprates. **a, Effective mass m^* of LSCO and Nd-LSCO as a function of doping, in units of the electron mass m_0 , for $p > p^*$. The value of m^* is obtained from specific heat data, via equation (2) (see Methods): in LSCO (green squares) at $p=0.26$ and 0.29 (ref. ³⁵), and at $p=0.33$ (ref. ³⁴); in Nd-LSCO (blue circles) at $p=0.24, 0.27, 0.36$ and 0.40 (ref. ³⁶). The solid line is a fit through the data, assumed to extend smoothly below $p=0.24$. **b**, Slope of the T -linear resistivity, plotted as $A_1^{\square}=A_1/d$, where d is the (average) distance between CuO_2 planes (see Methods): in LSCO (green squares) at $p=0.21, 0.23$ and 0.26 (Supplementary Section 7); in Nd-LSCO (blue circles) at $p=0.22$ and 0.23 under a pressure of 2 GPa to suppress the pseudogap phase (Fig. 1c and Supplementary Section 4) and $p=0.24$ at ambient pressure (Fig. 1a); in Bi2212 at $p=0.23$ (red hexagon, Fig. 2b). The experimental values are compared to the Planckian estimate (solid line) given by equation (1) with $\alpha=1.0$, namely $A_1^{\square}=(m^*/n)(k_B/e^2hd)=(h/2e^2T_F)$, using m^* from **a** (solid line in **a**) and $n=(1-p)/(a^2d)$ (Methods). For Nd-LSCO at $p=0.22$ and 0.23 , we assume that the pressure does not change the specific heat significantly above p^* . The error bars are explained in the Methods; the dotted lines represent the uncertainty on m^* .**

In LSCO, γ increases from $\gamma=6.9 \pm 1 \text{ mJ K}^{-2} \text{ mol}^{-1}$ at $p=0.33$ (ref. ³⁴) to $\gamma=14 \pm 2 \text{ mJ K}^{-2} \text{ mol}^{-1}$ at $p=0.26$ (ref. ³⁵), showing that m^* increases with reduced doping also in hole-doped cuprates (solid line in Fig. 3a). Applying equation (1) to LSCO data at $p=0.26$, using $n(a^2d)=1-p=0.74$ and $m^*=9.8 \pm 1.7 m_0$ (equation (2); Supplementary Table 1 in Supplementary Section 13), the Planckian limit predicts $A_1^{\square}=8.9 \pm 1.8 \Omega \text{ K}^{-1}$, while we see $A_1^{\square}=8.2 \pm 1.0 \Omega \text{ K}^{-1}$ (Fig. 1b and Supplementary Table 2 in Supplementary Section 13), so that $\alpha=0.9 \pm 0.3$ (Table 1).

In Nd-LSCO, an increase in m^* has also been observed in recent specific heat measurements³⁶, from $\gamma=5.4 \pm 1 \text{ mJ K}^{-2} \text{ mol}^{-1}$ at $p=0.40$ to $\gamma=11 \pm 1 \text{ mJ K}^{-2} \text{ mol}^{-1}$ at $p=0.27$ (Fig. 3a). At $p=0.24$, the electronic specific heat C_{el} varies as $C_{el}/T \sim \log(1/T)$, which complicates the estimation of m^* . Taking the mean value between $C_{el}/T=12 \text{ mJ K}^{-2} \text{ mol}^{-1}$ at 10 K and $C_{el}/T=22 \text{ mJ K}^{-2} \text{ mol}^{-1}$ at 0.5 K (ref. ³⁶), we get $m^*=12 \pm 4 m_0$ and hence $\alpha=0.7 \pm 0.4$, consistent with the Planckian limit for a third hole-doped material. See Table 1 for a summary of the numbers.

Finally, a stringent test of whether the Planckian limit operates in cuprates is provided by Bi2201, since in this particular cuprate

the pseudogap critical point that controls T -linear scattering occurs at a much higher doping than in other cuprates, namely $p^* \sim 0.4$ (see Supplementary Section 10). Despite this doubling of p^* and the very different volume of the Fermi surface relative to Bi2212, LSCO and Nd-LSCO, we find that $\alpha=1.0 \pm 0.4$ in Bi2201 (Table 1 and Supplementary Section 10).

In summary, our estimations reveal that the scattering rate responsible for the T -linear resistivity in PCCO, LCCO, Bi2212, LSCO, Nd-LSCO and Bi2201 tends to the same universal value, namely $h/\tau = \alpha k_B T$, with $\alpha=1.0$ (Table 1). A constant value of α in equation (1) implies that $A_1^{\square} \sim 1/T_F$, so that, in essence, $A_1^{\square} \sim m^*$. This explains why the slope of the T -linear resistivity is much larger in hole-doped than in electron-doped cuprates, since the effective mass is much higher in the former (Fig. 3a versus Fig. 4a). It also explains why A_1^{\square} increases in LSCO when going from $p=0.26$ to $p=0.21$ (Fig. 1b) and in Nd-LSCO (under pressure) when going from $p=0.24$ to $p=0.22$ (Fig. 1c). Indeed, as shown in Fig. 3, A_1^{\square} (Fig. 3b) and m^* (Fig. 3a) in LSCO and Nd-LSCO are seen to rise in tandem with decreasing p (we make the natural assumption that m^* continues to rise until p reaches p^* and that the pressure does

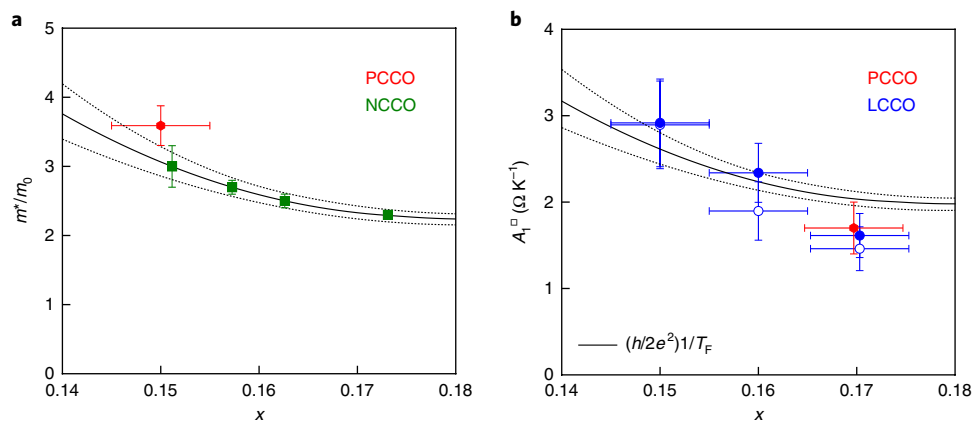


Fig. 4 | Effective mass m^* and slope of T -linear resistivity A_1^\square versus x in electron-doped cuprates. **a, Effective mass m^* of NCCO (green squares) as a function of doping, in units of m_0 , measured by quantum oscillations³⁰. Also shown is m^* of PCCO at $x=0.15$ (red hexagon), obtained from specific heat data³¹ (see Methods). For NCCO, the value of x is defined using the frequency F of quantum oscillations, via $F=(1-x)(h/2e^2)$. For PCCO, we use the nominal cerium content x , with its error bar (see Methods). The solid line is a fit through the NCCO data, assumed to extend smoothly below $x=0.15$. **b**, Slope of the T -linear resistivity, plotted as $A_1^\square=A_1/d$, where d is the distance between CuO_2 planes (Methods): in LCCO (blue) at $x=0.15, 0.16$ and 0.17 , both in a field (open circles, Fig. 1d) and in zero field (filled circles, Supplementary Section 6); in PCCO (red hexagon) at $x=0.17$ (Supplementary Section 5). The experimental values are compared to the Planckian estimate (solid line) given by equation (1) with $\alpha=1.0$, namely $A_1^\square=(m^*/n)(k_B/e^2\hbar d)$, using m^* from **a** (solid line in **a**) and $n=(1-x)/(a^2d)$ (Methods). The error bars are explained in the Methods; the dotted lines represent the uncertainty in m^* .**

not change the specific heat significantly above p^* in Nd-LSCO). Moreover, a Planckian limit on scattering provides an explanation for the ‘anomalous’ range in doping over which $\rho \sim A_1 T$ is observed in LSCO (ref. 8). As doping decreases below $p \sim 0.33$, scattering increases steadily until $p^* \sim 0.18$ – 0.19 , but the inelastic scattering rate $1/\tau$ cannot exceed the Planckian limit, reached at $p \sim 0.26$. Thus, between $p \sim 0.26$ and $p=p^*$, $\rho(T)$ is linear and $1/\tau$ saturates. The continuous increase of A_1 below $p \sim 0.26$ can be understood if we assume that m^* continues to increase in the range $p^* < p < 0.26$ (ref. 36), since $A_1 \sim m^*(1/\tau) \sim m^*$. If one could lower p^* , the range of T -linear resistivity would expand further. This is indeed what happens in Nd-LSCO when p^* is lowered by applying pressure¹² (Fig. 3b).

The fact that $\alpha \sim 1.0$ in cuprates has far-reaching implications since other metals with T -linear resistivity as $T \rightarrow 0$ also appear to have $\alpha \sim 1.0$ (ref. 10). The case is particularly clear in the organic conductor (TMTSF)₂PF₆, a well-characterized single-band metal whose resistivity is perfectly T -linear as $T \rightarrow 0$ (ref. 4), where $\alpha = 1.0 \pm 0.3$ (Table 1 and Supplementary Section 9). For such dramatically different metals as the quasi-1D organics and the cuprates—not to mention the heavy-fermion metals and the pnictides¹⁰—to all have quantitatively the same scattering rate in their respective T -linear regimes, there must be a fundamental and universal principle at play. Our findings support the idea^{9,10} that T -linear resistivity is achieved when the scattering rate hits the Planckian limit, given by $\hbar/\tau = k_B T$, whatever the scattering process, whether by antiferromagnetic spin fluctuations or not. If Planckian dissipation is the fundamental principle, new theoretical approaches are needed to understand how it works^{37–39}.

Online content

Any methods, additional references, Nature Research reporting summaries, source data, statements of data availability and associated accession codes are available at <https://doi.org/10.1038/s41567-018-0334-2>.

Received: 3 April 2018; Accepted: 28 September 2018;

Published online: 19 November 2018

References

- Löhneysen, H. v. et al. Non-Fermi-liquid behavior in a heavy-fermion alloy at a magnetic instability. *Phys. Rev. Lett.* **72**, 3262–3265 (1994).

- Fournier, P. et al. Insulator–metal crossover near optimal doping in $\text{Pr}_{2-x}\text{Ce}_x\text{CuO}_4$: Anomalous normal-state low temperature resistivity. *Phys. Rev. Lett.* **81**, 4720–4723 (1998).
- Grigera, S. A. et al. Magnetic field-tuned quantum criticality in the metallic ruthenate $\text{Sr}_3\text{Ru}_2\text{CuO}_7$. *Science* **294**, 329–332 (2001).
- Doiron-Leyraud, N. et al. Correlation between linear resistivity and T_c in the Bechgaard salts and the pnictide superconductor $\text{Ba}(\text{Fe}_{1-x}\text{Co}_x)_2\text{As}_2$. *Phys. Rev. B* **80**, 214531 (2009).
- Coleman, P. & Schofield, A. J. Quantum criticality. *Nature* **433**, 226–229 (2005).
- Martin, S. et al. Normal-state transport properties of $\text{Bi}_{2+x}\text{Sr}_{2-y}\text{CuO}_{6+\delta}$ single crystals. *Phys. Rev. B* **41**, 846–849 (1990).
- Daou, R. et al. Linear temperature dependence of resistivity and change in the Fermi surface at the pseudogap critical point of a high- T_c superconductor. *Nat. Phys.* **5**, 31–34 (2009).
- Cooper, R. A. et al. Anomalous criticality in the electrical resistivity of $\text{La}_{2-x}\text{Sr}_x\text{CuO}_4$. *Science* **323**, 603–607 (2009).
- Zaanen, J. Why the temperature is high. *Nature* **430**, 512–513 (2004).
- Bruin, J. A. N. et al. Similarity of scattering rates in metals showing T -linear resistivity. *Science* **339**, 804–807 (2013).
- Collignon, C. et al. Fermi-surface transformation across the pseudogap critical point of the cuprate superconductor $\text{La}_{1.6-x}\text{Nd}_{0.4}\text{Sr}_x\text{CuO}_4$. *Phys. Rev. B* **95**, 224517 (2017).
- Doiron-Leyraud, N. et al. Pseudogap phase of cuprate superconductors confined by Fermi surface topology. *Nat. Commun.* **8**, 2044 (2017).
- Jin, K. et al. Link between spin fluctuations and electron pairing in copper oxide superconductors. *Nature* **476**, 73–75 (2011).
- Sarkar, T. et al. Fermi surface reconstruction and anomalous low-temperature resistivity in electron-doped $\text{La}_{2-x}\text{Ce}_x\text{CuO}_4$. *Phys. Rev. B* **96**, 155449 (2017).
- Löhneysen, H. v. et al. Fermi-liquid instabilities at magnetic quantum phase transitions. *Rev. Mod. Phys.* **79**, 1015–1075 (2007).
- Dagan, Y. et al. Evidence for a quantum phase transition in $\text{Pr}_{2-x}\text{Ce}_x\text{CuO}_4$ from transport measurements. *Phys. Rev. Lett.* **92**, 167001 (2004).
- Tafti, F. F. et al. Nernst effect in the electron-doped cuprate superconductor $\text{Pr}_{2-x}\text{Ce}_x\text{CuO}_4$: superconducting fluctuations, upper critical field H_{c2} , and the origin of the T_c dome. *Phys. Rev. B* **90**, 024519 (2014).
- Motoyama, E. M. et al. Spin correlations in the electron-doped high-transition-temperature superconductor $\text{Nd}_{2-x}\text{Ce}_x\text{CuO}_4$. *Nature* **445**, 186–189 (2007).
- Matt, C. E. et al. Electron scattering, charge order, and pseudogap physics in $\text{La}_{1.6-x}\text{Nd}_{0.4}\text{Sr}_x\text{CuO}_4$: an angle-resolved photoemission spectroscopy study. *Phys. Rev. B* **92**, 134524 (2015).
- Yoshida, T. et al. Systematic doping evolution of the underlying Fermi surface of $\text{La}_{2-x}\text{Sr}_x\text{CuO}_4$. *Phys. Rev. B* **74**, 224510 (2006).
- Kaminski, A. et al. Change of Fermi-surface topology in $\text{Bi}_2\text{Sr}_2\text{CaCu}_2\text{O}_{8+\delta}$ with doping. *Phys. Rev. B* **73**, 174511 (2006).
- Benhabib, S. et al. Collapse of the normal-state pseudogap at a Lifshitz transition in the $\text{Bi}_2\text{Sr}_2\text{CaCu}_2\text{O}_{8+\delta}$ cuprate superconductor. *Phys. Rev. Lett.* **114**, 147001 (2015).

23. Hussey, N. E. et al. Phenomenology of the normal-state in-plane transport properties of high- T_c cuprates. *J. Phys. Condens. Matter* **20**, 123201 (2008).
24. Fauqué, B. et al. Dispersion of the odd magnetic resonant mode in near-optimally doped $\text{Bi}_2\text{Sr}_2\text{CaCu}_2\text{O}_{8+\delta}$. *Phys. Rev. B* **76**, 214512 (2007).
25. Tranquada, J. M. et al. Coexistence of, and competition between, superconductivity and charge-stripe order in $\text{La}_{1.62-x}\text{Nd}_{0.4x}\text{Sr}_x\text{CuO}_4$. *Phys. Rev. Lett.* **78**, 338 (1997).
26. Hussey, N. E. et al. Generic strange metal behavior of overdoped cuprates. *J. Phys. Conf. Series* **449**, 012004 (2013).
27. Hayes, I. M. et al. Scaling between magnetic field and temperature in the high-temperature superconductor $\text{BaFe}_2(\text{As}_{1-x}\text{P}_x)_2$. *Nat. Phys.* **12**, 919 (2016).
28. Matsui, H. et al. Evolution of the pseudogap across the magnet-superconductor phase boundary of $\text{Nd}_{2-x}\text{Ce}_x\text{CuO}_4$. *Phys. Rev. B* **75**, 224514 (2007).
29. Helm, T. et al. Evolution of the Fermi surface of the electron-doped high-temperature superconductor $\text{Nd}_{2-x}\text{Ce}_x\text{CuO}_4$ revealed by Shubnikov-de Haas oscillations. *Phys. Rev. Lett.* **103**, 157002 (2009).
30. Helm, T. et al. Correlation between Fermi surface transformations and superconductivity in the electron-doped high- T_c superconductor $\text{Nd}_{2-x}\text{Ce}_x\text{CuO}_4$. *Phys. Rev. B* **92**, 094501 (2015).
31. Yu, W. et al. Magnetic-field dependence of the low-temperature specific heat of the electron-doped superconductor $\text{Pr}_{1.85}\text{Ce}_{0.15}\text{CuO}_4$. *Phys. Rev. B* **72**, 212512 (2005).
32. Bangura, A. et al. Fermi surface and electronic homogeneity of the overdoped cuprate superconductor $\text{Tl}_2\text{Ba}_2\text{CuO}_{6+\delta}$ as revealed by quantum oscillations. *Phys. Rev. B* **82**, 140501R (2010).
33. Loram, J. W. et al. Evidence on the pseudogap and the condensate from the electronic specific heat. *J. Phys. Chem. Solids* **62**, 59–64 (2001).
34. Nakamae, S. et al. Electronic ground state of heavily overdoped nonsuperconducting $\text{La}_{2-x}\text{Sr}_x\text{CuO}_4$. *Phys. Rev. B* **68**, 100502R (2003).
35. Wang, Y. et al. Weak-coupling d -wave BCS superconductivity and unpaired electrons in overdoped $\text{La}_{2-x}\text{Sr}_x\text{CuO}_4$ single crystals. *Phys. Rev. B* **76**, 064512 (2007).
36. Michon, B. et al. Thermodynamic evidence of quantum criticality in cuprate superconductors. Preprint at <https://arxiv.org/abs/1804.08502> (2018).
37. Davison, R. A., Schalm, K. & Zaanen, J. Holographic duality and the resistivity of strange metals. *Phys. Rev. B* **89**, 245116 (2014).
38. Hartnoll, S. A. Theory of universal incoherent metallic transport. *Nat. Phys.* **11**, 54–61 (2015).
39. Song, X. Y. et al. Strongly correlated metal built from Sachdev-Ye-Kitaev models. *Phys. Rev. Lett.* **119**, 216601 (2017).
41. Charpentier, S. et al. Antiferromagnetic fluctuations and the Hall effect of electron-doped cuprates: possibility of a quantum phase transition at underdoping. *Phys. Rev. B* **81**, 104519 (2010).
42. Hussey, N. E. et al. Dichotomy in the T -linear resistivity in hole-doped cuprates. *Phil. Trans. R. Soc. A* **369**, 1626–1639 (2011).

Acknowledgements

The authors would like to thank K. Behnia, C. Bourbonnais, R. Greene, S. Hartnoll, N. Hussey, M.-H. Julien, D. Maslov, J. Paglione, S. Sachdev, A.-M. Tremblay and J. Zaanen for fruitful discussions. A portion of this work was performed at the LNCMI, a member of the European Magnetic Field Laboratory (EMFL). C.P. acknowledges funding from the French ANR SUPERFIELD, and the LABEX NEXT. P.F. and L.T. acknowledge support from the Canadian Institute for Advanced Research (CIFAR) and funding from the Natural Sciences and Engineering Research Council of Canada (NSERC), the Fonds de recherche du Québec - Nature et Technologies (FRQNT) and the Canada Foundation for Innovation (CFI). L.T. acknowledges support from a Canada Research Chair. This research was undertaken thanks in part to funding from the Canada First Research Excellence Fund. Part of this work was funded by the Gordon and Betty Moore Foundation's EPiQS Initiative (grant GBMF5306 to L.T.).

Author contributions

A.L., S.B., W.T., B.V., D.V. and C.P. performed the transport measurements at the LNCMI. A.L., F.L., M.L. and N.D.-L. performed the transport measurements at Sherbrooke. H.R., P.A.-S. and Z.Z.L. prepared the Bi2212 film, which was then characterized by A.L., H.R., P.A.-S., Z.Z.L. and D.C. M.D. and P.F. prepared and characterized the PCCO films. A.L., F.L., L.T. and C.P. wrote the manuscript, in consultation with all authors. L.T. and C.P. co-supervised the project.

Competing interests

The authors declare no competing interests.

Additional information

Supplementary information is available for this paper at <https://doi.org/10.1038/s41567-018-0334-2>.

Reprints and permissions information is available at www.nature.com/reprints.

Correspondence and requests for materials should be addressed to L.T. or C.P.

Publisher's note: Springer Nature remains neutral with regard to jurisdictional claims in published maps and institutional affiliations.

© The Author(s), under exclusive licence to Springer Nature Limited 2018

Methods

Samples. Bi2212. Our thin film of $\text{Bi}_2\text{Sr}_2\text{CaCu}_2\text{O}_{8+\delta}$ (Bi2212) was grown epitaxially at 740 °C on a SrTiO_3 substrate by radiofrequency magnetron sputtering with O_2/Ar gas and fully oxygen overdoped after deposition⁴⁰. The film thickness was measured by deposition rate calibration, giving $t = 240 \pm 15$ nm. The film was patterned by mechanical scribing (avoiding the need for a lithography resist) into the shape of a Hall bar consisting of two large pads (for current) connected by a narrow bridge (275 μm wide) between 2 couples of voltage pads distant by 1.15 mm for longitudinal and transverse resistance measurements. Six gold contacts were deposited by sputtering on the different pads and gold wires were attached with silver paint.

The superconducting transition temperature $T_c = 50$ K was determined as the temperature below which the zero-field resistance $R = 0$. The hole doping p is obtained from T_c , using the usual convention^{21,22}, according to which our overdoped sample has a nominal doping $p = 0.23$. This means that its doping is just slightly above the end of the pseudogap phase²² (see Supplementary Section 2). It is also just above the Lifshitz transition where its anti-bonding band crosses the Fermi level to produce an electron-like diamond-shaped Fermi surface²¹ (see Supplementary Section 1).

PCCO. Our thin films of $\text{Pr}_{2-x}\text{Ce}_x\text{CuO}_{4+\delta}$ (PCCO) were grown by pulsed laser deposition on LSAT substrates under 200 mTorr of N_2O using targets including an excess of Cu to suppress the growth of parasitic phases⁴¹. Films were then annealed for 4 min in vacuum. The film thickness was measured via the width of X-ray diffraction peaks, giving $t = 230 \pm 30$ nm. A very small amount of parasitic phase was detected in the X-ray diffraction spectra. However, its impact on the cross-section of the films should be much smaller than the uncertainty coming from the thickness measurement. Six indium–silver contacts were applied in the standard geometry.

The superconducting transition temperature $T_c = 13$ K was determined as the temperature below which the zero-field resistance $R = 0$. The electron concentration is taken to be the cerium content, $x = 0.17$, with an error bar ± 0.005 . This means that our samples have a concentration slightly above the quantum critical point where the Fermi surface of PCCO is known to undergo a reconstruction by antiferromagnetic ordering¹⁶. The Fermi surface of NCCO at that doping could not be simpler: it is a single circular cylinder²⁸ (see Supplementary Section 1).

Measurement of the longitudinal and transverse resistances. The longitudinal resistance R_{xx} and transverse (Hall) resistance R_{xy} of our Bi2212 film were measured in Toulouse in pulsed fields up to 58 T. The measurements were performed using a conventional 6-point configuration with a current excitation of 0.5 mA at a frequency of ~ 10 kHz. A high-speed acquisition system was used to digitize the reference signal (current) and the voltage drop across the sample at a frequency of 500 kHz. The data were post-analysed with software to perform the phase comparison. Data for the rise and fall of the field pulse were in good agreement, thus excluding any heating due to eddy currents. Tests at different frequencies showed excellent reproducibility.

R_{xx} and R_{xy} of our Bi2212 film were also measured in Orsay, at $H = 0$ and $H = 9$ T, respectively.

The longitudinal resistance R_{xx} values of our three PCCO films were measured in Sherbrooke in a zero field and in a steady field of 16 T.

Values of m^* and A_1 . *Hole-doped cuprates.* The values of p and m^* used in Fig. 3a are listed in Supplementary Table 1 (see Supplementary Section 13). For Nd-LSCO, the value of p with its error bar is taken from ref. 11. For LSCO, the value of p is taken from refs 34,35, and we assume the same error bar as for Nd-LSCO. The value of m^* is obtained from the measured specific heat γ , via equation (2). For Nd-LSCO, the value of γ with its error bar is taken from ref. 36, except for $p = 0.24$, where we take the average between the electronic specific heat C_e/T at $T = 10$ K (12 $\text{mJ K}^{-2} \text{mol}^{-1}$) and at $T = 0.5$ K (22 $\text{mJ K}^{-2} \text{mol}^{-1}$), given that C_e/T is not constant at low T (ref. 36). For Bi2212 and LSCO, we estimate γ and its error bar from the data published in ref. 33 and in refs 34,35, respectively (see Supplementary Section 8). With these values of m^* , we calculate $T_F = (\pi\hbar^2/k_B)(nd/m^*)$, using $n = (1-p)/(a^2d)$ since the Fermi surface of Bi2212, LSCO and Nd-LSCO is electron-like at the dopings considered here (see Supplementary Section 1). We then obtain the Planckian limit on the resistivity slope, namely $A_1^{\square} = h/(2e^2T_F)$, whose values are listed in the last column of Supplementary Table 2 (see Supplementary Section 13) and plotted in Fig. 3b (solid black line). For Bi2201, the values of n , m^* and A_1 are given in Supplementary Section 10, with associated error bars and references.

The values of p and A_1 used in Fig. 3b are listed in Supplementary Table 2 (see Supplementary Section 13). For Nd-LSCO, the value of p with its error bar is taken from ref. 11. For LSCO, the value of p is taken from refs 8,42, and we assume the same error bar as for Nd-LSCO. For Nd-LSCO, the value of A_1 is obtained from a linear fit to the raw data in Fig. 1a ($p = 0.24$, at $H = 16$ T) and in Fig. 1c ($p = 0.22$ and 0.23 , at $H = 33$ T and $P = 2$ GPa). Note that the magnetoresistance is very weak in Nd-LSCO. For example, at $p = 0.24$, $A_1 = 0.47 \mu\Omega \text{cm K}^{-1}$ at $H = 33$ T (Fig. 1c) versus $A_1 = 0.49 \mu\Omega \text{cm K}^{-1}$ at $H = 16$ T (Fig. 1a). For LSCO, the value of A_1 is obtained from a linear fit to the raw data in Fig. 1b ($p = 0.26$, at $H = 18$ T) and to the magnetoresistance-corrected data in Supplementary Section 7 ($p = 0.21$ and 0.23). Note that the magnetoresistance in LSCO does not significantly change the slope A_1 (Fig. 1b versus Supplementary Fig. 7). For Bi2212, the value of A_1 is obtained from a linear fit to magnetoresistance-corrected data (Fig. 2b and Supplementary Section 3). The error bar on A_1 is in all cases taken to be $\pm 10\%$, the estimated uncertainty in measuring the geometric factor of small samples. The values of A_1 listed in Supplementary Table 2 (see Supplementary Section 13) are used to obtain the experimental values of $A_1^{\square} = A_1/d$ that are plotted in Fig. 3b.

Electron-doped cuprates. The values of x and m^* used in Fig. 4a are listed in Supplementary Table 3 (see Supplementary Section 13). For NCCO, the value of x is obtained from the frequency F of quantum oscillations, measured precisely^{29,30} (see Supplementary Section 1), via $x = 1 - (2eFa^2/h)$. The value of m^* is obtained directly from the high-frequency quantum oscillations, as reported (with error bar) in refs 29,30. At the lowest doping (for example, $x = 0.15$), the Fermi surface of NCCO is reconstructed by an antiferromagnetic order leading to small electron and hole pockets. The small gap between the pockets decreases as the doping increases and, at $x = 0.17$, angle-resolved photoemission spectroscopy data show that the large hole-like Fermi surface is recovered²⁸. At doping levels $x = 0.151$ to 0.163 , we assume that the effective mass of the high quantum oscillation frequency due to magnetic breakdown is representative of the large hole-like Fermi surface, as expected in semiclassical theory⁴³. The continuous trend of decreasing effective mass in the doping range $x = 0.151$ to 0.163 is confirmed by the smaller (and smoothly connected) value at $x = 0.173$.

For PCCO, x is taken to be the cerium content, with an error bar ± 0.005 . Here m^* is obtained from the measured specific heat γ , via equation (2), and the value of γ (with its error bar) is taken from ref. 31. With these values of m^* , we calculate $T_F = (\pi\hbar^2/k_B)(nd/m^*)$, using $n = (1-x)/(a^2d)$ since the Fermi surface of NCCO and PCCO is hole-like (see Supplementary Section 1). The good agreement between the specific heat data in PCCO at $x = 0.15$ and the values of the effective mass in NCCO (Fig. 4a) further confirms the validity of our approach regarding the extraction of m^* .

We then obtain the Planckian limit on the resistivity slope, namely $A_1^{\square} = h/(2e^2T_F)$, whose values are listed in the last column of Supplementary Table 3 (see Supplementary Section 13) and plotted in Fig. 4b (solid black line).

The values of x and A_1 used in Fig. 4b are listed in Supplementary Table 4 (see Supplementary Section 13). In all cases, x is taken to be the cerium content, with an error bar ± 0.005 . For PCCO at $x = 0.17$, the value of A_1 is obtained from a linear fit to the raw data in Supplementary Section 5. Within error bars, the same value is measured in all three PCCO films, whether at $H = 0$ or at $H = 16$ T. For LCCO, the value of A_1 is obtained from a linear fit to the raw data in Fig. 1d. Also listed in Supplementary Table 4 (see Supplementary Section 13) are the values of A_1 obtained from a linear fit to the raw zero-field data in LCCO (see Supplementary Section 6). The error bar on A_1 is $\pm 15\%$ for our PCCO film, the uncertainty in measuring the film thickness. We apply the same error bar for LCCO. The values of A_1 listed in Supplementary Table 4 (see Supplementary Section 13), both in zero field and in finite field, are used to obtain the experimental values of $A_1^{\square} = A_1/d$ that are plotted in Fig. 4b (as filled and open circles, respectively).

Data availability

The data that support the plots within this paper and other findings of this study are available from the corresponding authors (L.T. or C.P.) upon reasonable request.

References

- Konstantinovic, Z., Li, Z. Z. & Raffy, H. Temperature dependence of the Hall effect in single-layer and bilayer $\text{Bi}_2\text{Sr}_2\text{Ca}_{1-x}\text{Cu}_n\text{O}_y$ thin films at various oxygen contents. *Phys. Rev. B* **62**, R11989(R) (2000).
- Falicov, L. M. & Stachowiak, H. Theory of the de Haas–van Alphen effect in a system of coupled orbits. Application to magnesium. *Phys. Rev.* **147**, 505 (1966).